HHS Public Access

Author manuscript

Methods Enzymol. Author manuscript; available in PMC 2020 May 16.

Published in final edited form as:

Methods Enzymol. 2017 ; 582: 193–219. doi:10.1016/bs.mie.2016.08.005.

Single-Stranded DNA Curtains for Studying Homologous Recombination

C.J. Ma[1], **J.B. Steinfeld**[1], **E.C. Greene**[2]

Columbia University, New York, NY, United States

Abstract

Homologous recombination is an important pathway involved in the repair of double-stranded DNA breaks. Genetic studies form the foundation of our knowledge on homologous recombination. Significant progress has also been made toward understanding the biochemical and biophysical properties of the proteins, complexes, and reaction intermediates involved in this essential DNA repair pathway. However, heterogeneous or transient recombination intermediates remain extremely difficult to assess through traditional ensemble methods, leaving an incomplete mechanistic picture of many steps that take place during homologous recombination. To help overcome some of these limitations, we have established DNA curtain methodologies as an experimental platform for studying homologous DNA recombination in real-time at the single-molecule level. Here, we present a detailed overview describing the preparation and use of single-stranded DNA curtains in applications related to the study of homologous DNA recombination with emphasis on recent work related to the study of the eukaryotic recombinase Rad51.

1. INTRODUCTION

1.1 Homologous Recombination

Homologous recombination (HR) is a highly conserved pathway that enables the exchange of genetic information between identical or closely related DNA molecules, and is an important driving force in genome evolution. HR plays crucial roles in the repair of double-stranded DNA breaks (DSBs), the rescue of stalled or collapsed replication forks, chromosomal rearrangements, horizontal gene transfer, and meiosis in sexually reproducing organisms (Cromie, Connelly, & Leach, 2001; Heyer, Ehmsen, & Liu, 2010; San Filippo, Sung, & Klein, 2008; Sasaki, Lange, & Keeney, 2010).

Much of our knowledge of HR comes from the study of DSB repair in the budding yeast *Saccharomyces cerevisiae* (Haber, 2012; Paques & Haber, 1999; Symington, Rothstein, & Lisby, 2014). Here, we briefly highlight some of the key steps and proteins involved during the early stages of DSB repair in *S. cerevisiae* (Fig. 1); for a more in-depth discussion of HR, we refer the reader to several excellent reviews (Heyer et al., 2010; San Filippo et al., 2008; Symington et al., 2014). Upon formation of a DSB the newly liberated DNA ends are processed to yield long 3′ single-stranded DNA (ssDNA) overhangs. Replication protein A

[2]Corresponding author: ecg2108@columbia.edu.

[1]Equal contribution.

(RPA) binds to these overhang to remove any potential secondary structure and also protect the ssDNA from degradation by nucleases. RPA is then replaced, with the help of mediators such as Rad52, by the recombinase Rad51, an ATP-dependent DNA-binding protein that forms an extended right-handed helical filament on the ssDNA overhang (Bianco, Tracy, & Kowalczykowski, 1998; Morrical, 2015). This nucleoprotein filament, referred to as the presynaptic complex, is responsible for aligning and pairing the ssDNA overhang with a homologous double-stranded DNA (dsDNA) sequence present elsewhere in the genome. The 3′ end of the presynaptic ssDNA can prime replication using homologous dsDNA as a template and the resulting intermediates can be channeled through a number of distinct pathways that will restore the originally broken DNA molecule (Heyer et al., 2010; San Filippo et al., 2008; Symington et al., 2014).

The highly simplified view of HR presented earlier belies the fact that recombination requires the coordinated action of a complex repertoire of proteins. Highly organized macromolecular assemblies are responsible for sensing DNA damage, recruiting essential factors to the damaged sites, and repairing the damaged DNA. Many of these proteins belong to the RAD52 epistasis group of genes, which were initially identified in *S. cerevisiae* as mutants that exhibited extreme sensitivity to ionizing radiation (Game & Mortimer, 1974), and many other HR proteins have been identified in subsequent years. In total, at least 45 different proteins are known to be directly involved DSB repair in *S. cerevisiae* (Symington et al., 2014).

Genetic experiments have provided the basis for most of the current body of knowledge in HR and continue to yield important new insights (Paques & Haber, 1999; Symington et al., 2014). Cell biology studies have also yielded an enormous amount of information regarding the protein and DNA components involved in eukaryotic HR (Lisby & Rothstein, 2009, 2015; Mine-Hattab & Rothstein, 2013). Biochemical and biophysical studies have been employed to study several aspects of the reaction, and these experiments have revealed some crucial insights into HR mechanisms (Bianco et al., 1998; Morrical, 2015). More recently, structural approaches have unveiled atomic-level details of some proteins and protein-DNA complexes that are essential to HR (Chen, Yang, & Pavletich, 2008; Conway et al., 2004). However, many questions related to the HR mechanisms cannot be addressed through any of these types of approaches because the underlying intermediates are either transient or heterogeneous. Single-molecule fluorescence-based methods offer the potential for direct visual analysis of individual HR reaction components or complexes, which in turn can enable the direct detection of subpopulations within an otherwise heterogeneous mixture and can also capture rare or transient intermediates along a reaction trajectory.

1.2 Single-Molecule Biology

Single-molecule approaches are technically demanding, and it is relevant to ask whether it is worth the trouble to study complex biological systems at the scale of individual components. As an analogy, take the study of salmon swimming upstream to spawn. One could tag 1000 salmon at a river inlet, and then wait upstream to determine, for instance, how many fish reached their spawning grounds, how long it took them to get there, and how many fish actually spawned. Such a study would provide valuable information about the salmon

population and basic insight into their life cycle. However, the study as presented could not answer why some salmon survived and some did not, what factors dictate precise arrival time, or why some salmon successfully spawn whereas others do not. To address these types of questions, the study must be redesigned to follow individual fish within the population as they swim toward the spawning grounds. Through this type of study, one might find that some salmon were harvested by anglers or bears, others may be unable to navigate fish ladders, and still others may have experienced too much stress during their travels to spawn successfully. Suddenly, the picture of salmon reproduction becomes much more detailed. Similarly, ensemble biochemical or genetic studies typically can look only at some well-defined intermediate state or the final output from a process, and may overlook heterogeneous intermediates or transient states that are important for understanding the overall nature a particular reaction. Experimental approaches capable of interrogating individual macromolecules or complexes over the course of a biochemical reaction trajectory now offer new possibilities for understanding many types of biological problems in greater depth than previously possibly.

1.3 Overview of DNA Curtains

Two challenges users of single-molecule methods face are the difficulties associated with collecting statistically relevant information and the problem of nonspecific surface absorption, which arises because most single-molecule bases methods require that the biomolecules under investigation be anchored to a solid supporting surface without compromising biological activity. To help overcome these problems we have developed "DNA curtains," in which ds- or ssDNA molecules can be organized into defined patterns on the surface of a microfluidic sample chamber (Fig. 2) (Fazio, Visnapuu, Wind, & Greene, 2008; Gorman, Fazio, Wang, Wind, & Greene, 2010; Gorman, Plys, Visnapuu, Alani, & Greene, 2010; Graneli, Yeykal, Prasad, & Greene, 2006). In brief, DNA curtains are prepared by first depositing metal barriers and anchors on the surface of a fused silica microscope slide by electron beam (e-beam) lithography. The slide is then coated with a fluid lipid bilayer, which prevents nonspecific surface adsorption and provides a mobile platform for anchoring DNA molecules through a biotin-streptavidin linkage. Buffer flow is then used to push the DNA molecules into the barriers where they all align with one another (Fazio et al., 2008; Graneli et al., 2006). If desired, the second end of the DNA can be attached to a downstream anchor point (Gorman, Fazio, et al., 2010; Gorman, Plys, et al., 2010). This approach allows for the direct observation of hundreds of individual DNA molecules within the typical field of view of an optical microscope, providing a flexible experimental platform that can be used to study different types of protein-DNA interactions (Duzdevich et al., 2015; Gorman, Fazio, et al., 2010; Gorman, Plys, et al., 2010; Gorman et al., 2012; Lee, Finkelstein, Arciszewska, Sherratt, & Greene, 2014; Lee et al., 2015; Qi et al., 2015; Redding et al., 2015; Silverstein, Gibb, & Greene, 2014; Sternberg, Redding, Jinek, Greene, & Doudna, 2014; Wang et al., 2013). In subsequent sections, we describe how to prepare ssDNA curtains (Gibb, Silverstein, Finkelstein, & Greene, 2012) and provide brief examples of how this technique has been applied to the study of HR with emphasis on recent experiments using the eukaryotic DNA recombinase Rad51 (Lee et al., 2015; Qi et al., 2015).

2. METHODS

We use total internal reflection fluorescence microscopy (TIRFM) for visualizing DNA curtains. TIRFM uses spatially selective laser excitation to reduce background signal by several orders of magnitude relative to conventional wide-field illumination techniques (Axelrod, 1989). Detailed descriptions of TIRF microscopes are widely available, and below provide a component list describing our most recent instruments, which uses inverted Nikon Eclipse microscopes equipped with custom laser illumination systems for dual-color prism-type TIRFM illumination (Fig. 3).

2.1 Instrumentation

Microscope body	Nikon Eclipse Ti-E with Perfect Focus System (PFS)
Camera	Two Andor iXon X_3 EMCCDs (Model: DU-897E-C50-#BV)
Objective	Nikon CFI PLAN APO 60X WI
Filter cube	Chroma TE2000/Ti filter cube (Part No. 91020)
	Chroma ET525/50 m band pass filter
	Chroma ET575lp long pass filter
	Chroma ZT561rdc dichroic mirror
Illumination	Coherent Sapphire LP (488 nm, 200 mW)
	Coherent Sapphire LP (561 nm, 200 mW)
	Chroma ZT488rde-UF1 dichroic
TIRF prism	Thor Labs, custom-made, uncoated, fused silica
Shutter	Vincent Associates Uniblitz VCM-D1 Single Channel Uni-Stable Shutter
Objective heater	Bioptech Objective Heater Controller (150803) and Standard heater (150819–19)
Slide heater	Custom made aluminum casing with Omega Mini Benchtop Controller (CSC32J)

2.2 Flow Cell Fabrication

Our DNA curtain experiments are performed using flow cells that are machined and assembled in-house (Fig. 4). In brief, each flow cell is made from a fused silica microscope slide. Inlet and outlet holes are bored into each slide using a diamond-coated drill bit. Metallic patterns are deposited on the surface of the slide by e-beam lithography, and the patterns can be designed for either single- or double-tethered formats. These modified slides are then cleaned and assembled into the flow cells that are used for making DNA curtains. Later, we summarize each of these procedures, and detailed explanations of each step have also been previously published (Greene, Wind, Fazio, Gorman, & Visnapuu, 2010).

2.2.1 Slide Preparation—First, two holes are cut through each fused silica slide to allow sample delivery in the completed flow cell (Fig. 4). The holes are drilled using a 1.4-mm diamond-coated drill bit (Shor International, Cat. No. DIB-211.00). While drilling, the slides are submerged in a water bath to cool the bit and prevent inhalation of fused silica dust (Greene et al., 2010).

The drilled slides are then cleaned by submersion in piranha solution (3:1 mixture of concentrated sulfuric acid (97%) and 30% hydrogen peroxide). For cleaning, up to 10 slides are placed in a glass slide rack and the rack is placed within rectangular glass staining dish (e.g., Electron Microscopy Sciences, Cat. No. 70312–20). The dish is then filled with 150 mL of sulfuric acid followed by the addition of 50 mL cold hydrogen peroxide. The slides are incubated in the piranha solution for 30 min. Extreme care must be taken when handling piranha solution to avoid contact with exposed skin. Following the 30-min submersion in piranha solution, the slides should be rinsed with copious amounts of deionized water.

The cleaned and drilled slides must now be prepped for lithography by deposition of a positive photoresist and conductive polymer layer (Fig. 4A). For this, the slides are spin-coated with a layer of 3% (w/v) polymethylmethacrylate (PMMA; molecular weight 25 kDa), dissolved in anisole (MicroChem, Newton, MA), followed by a layer of 1.5% (w/v) PMMA (495 kDa), also dissolved in anisole. The PMMA layers are then topped off with a final layer of AquaSAVE conducting polymer (Mitsubishi Rayon, Tokyo, Japan). Each of these layers is spun at 4000 rpm for 45 s using a ramp rate of 300 rpm/s using a Laurell Technologies Corp spincoater (WS-650MZ-23NPP).

The slides are now ready for e-beam lithography. We use an FEI scanning transmission electron microscope equipped with nano pattern generator system software (Nabity, Inc.), which controls the e-beam as it writes patterns on coated fused silica slides. Dosage tests can be used to determine the current and writing time that yield the best combination of time and resolution for the desired patterns. The slides are then developed to remove the PMMA from the areas exposed to the e-beam. This step is performed by placing the slide within a 50-mL falcon tube containing a developing solution comprised of a 3:1 mixture of methyl isobutyl ketone:isopropanol cooled to −20°C. The tube is sonicated in an icy water bath sonicator (Branson 1800, power LOW, 60 s processing time), and rinsed off with isopropyl alcohol (IPA). A thin layer of chrome (~20-nm) is then deposited onto the patterned surfaces using a Semicore E-beam Evaporation System (SC 2000LT). The remaining PMMA is then removed by first washing the slides with acetone from a squirt bottle. The slides are then submerged in acetone and sonicated for 5–10 min. Finally, the patterned slides are rinsed with clean acetone from a wash bottle. To prevent formation of deposits from the acetone drying, acetone is cleaned away with IPA and dried with a stream of nitrogen gas.

2.2.2 Flow Cell Assembly and Disassembly—Prior to use, the patterned slides must be assembled into flow cells that can be connected to a sample deliver system (Fig. 4B and C). The flow cells are made by using double-sided tape to create a sample chamber between the patterned slide and a glass coverslip. Later we provide a step-by-step description of the flow cell assembly procedure, as well as information describing how the flow cells can be dismantled and reused.

1. Center a rectangular paper template (35 × 5 mm) over a piece of double-sided tape (19 mm width) and tape over the chrome pattern on the slide.
2. Use the paper template as a guide to excise a channel in the double-sided tape.

3. Place a coverslip (Fisher Scientific, Fisher Finest Premium cover glass, Cat. No. 12-548-5E) on top of the tape and apply pressure to seal the coverslip to the tape.
4. The assembled flow cell is sandwiched between glass slides (Fisher Scientific, Frosted microscope slides 12-550-343) and held by binder clips on all four sides to distribute pressure evenly.
5. Bake the assembly under vacuum for 45 min at 140°C to seal the tape.
6. Remove from the oven, release the binder clips and the glass slides.
7. Glue Nanoports (Idex, Cat. No. N-333) over the drilled port holes with a hot glue gun. The flow cell is now complete and can be stored under vacuum at room temperature until use.
8. Patterned slides can be reused after each experiment. Submerge the slide in ethanol for ~48 h, and then remove the ports, coverslip, and double-sided tape. The slides are then cleaned by submersion in the following solutions with constant stirring: 2% Hellmanex solution for 48 h; rinse with Milli-Q water; 1 *M* NaOH for 40 min, rinse with Milli-Q water; 100% ethanol for 30 min. The cleaned slides are then ready for reuse.

2.3 ssDNA Curtains

The assembled flow cells can now be used for the preparation of the ssDNA curtains. First, a lipid bilayer is used to passivate the flow cell surface. The ssDNA substrate is then attached to the lipid bilayer through a biotin-streptavidin-biotin linkage, and buffer flow is used to push the anchored ssDNA molecules into position along the chrome barriers. Finally, the ssDNA is labeled and extended by injecting fluorescently tagged RPA into the sample chamber. The following sections provide step-by-step details necessary to complete each of these procedures.

2.3.1 Liposome Preparation

1. Lipid stocks are prepared by dissolving the following components in 10 mL of chloroform: 1 g DOPC (1,2-dioleoyl-*sn*-glycero-3-phosphocholine), 100 mg PEG-2000 DOPE (18:1 PEG-2000: 1,2-dioleoyl-*sn*-glycero-3-phosphoethanolamine-*N*-[methoxy (polyethylene glycol)-2000] (ammonium salt)), 5 mg biotinylated DOPE. The dissolved lipid mixtures can then be stored at −20°C. All lipids are purchased from Avanti Polar Lipids, Inc.
2. The lipid stock solutions are used to make liposomes. Liposomes are typically prepared in 2 mL batches, using the following step-by-step procedure, and can stored at 4°C for 4–8 weeks.
    i. Clean an organic-solvent compatible syringe with chloroform and transfer 200 μL (1/10th of the final desired volume) of the lipid stock to a new 2-mL glass vial (National Scientific, Cat. No. C4015).
    ii. Using a very low pressure stream of nitrogen gas, evaporate the chloroform from the lipid stock slowly over several minutes. During

this time, the lipid stock will form a solid residue on the side of the vial. After all the chloroform is evaporated, slightly increase the pressure and continue blowing nitrogen until all traces of liquid are removed.

iii. Place the uncapped glass vial under vacuum overnight.

iv. Add 2 mL of lipid buffer (10 m*M* Tris-HCl [pH 8.0], 100 m*M* NaCl) to the dried lipid stock and cap the vial. Incubate at room temperature for an hour and then vortex until all the lipid stock has dissolved into solution.

v. Transfer the mixture to a 5-mL polypropylene culture tube (Falcon, Cat. No. 35–2058) and sonicate in an ice bath using a microtip sonicator (Misonix S-4000) until the solution becomes clear.

vi. The solution is then filtered through a 0.22-μm nylon syringe filer (Fisherbrand, Cat. No. 09-720-3) and the resulting liposomes are ready for use.

2.3.2 Preparation of ssDNA—Our ssDNA curtain experiments make use of relative long ssDNA substrates (≥40,000 nucleotides) that are made by rolling circle replication with a biotinylated oligonucleotide primer and a circular ssDNA template (Gibb et al., 2012), as described later.

1. The biotinylated primer is first annealed to a circular M13 DNA template in a 100-μL reaction containing: 40 m*M* Tris-HCl [pH 8.0], 50 m*M* NaCl, 10 m*M* $MgCl_2$, 10 μg (89.4 n*M*) of M13mp18 (New England Biolabs, Cat. No. N4040S), and 45 n*M* primer (5′-BIO-TEG-TTT TTT TTT TTT TTT TTT TTT TTT TTT TTT GTA AAA CGA CGG CCA GT). The sample is placed in near boiling water (~95°C) in a 1-L beaker for 5 min, and the beaker is then transferred to the benchtop and allowed to cool slowly to room temperature. The annealing reactions are then in buffer containing 10 m*M* Tris-HCl [pH 8.0], 50 m*M* NaCl, and 5 m*M* $MgCl_2$ to a total volume of 300 μL and stored at −20°C until use.

2. A fresh preparation of ssDNA is made for each ssDNA curtain experiment. Rolling circle reactions (50 μL) are prepared containing: 10 μL of 5 × reaction buffer (250 m*M* Tris-HCl [pH 7.5]), 20 m*M* DTT, 50 m*M* ammonium sulfate, and 50 m*M* $MgCl_2$), 1 μL annealed M13 template (see earlier), 1 μL of 10 m*M* dNTP mix, 1 μL purified ϕ29 polymerase (10 μ*M* stock) (Gibb et al., 2012), and 37 μL water. Mix by pipetting, do not vortex. Incubate at 30°C for 25 min, and use immediately after preparation.

2.3.3 Lipid Bilayer Deposition and ssDNA Attachment—The following section describes how the bilayer is deposited onto the flow cell surface and how the ssDNA substrate is attached to the bilayer. These steps are all performed manually at the benchtop using hand held syringes. Extreme care should be taken to prevent any air from entering the flow cell once the bilayer has been deposited, and all tubing and syringe attachments should be made using drop-to-drop connections. If air bubbles pass through the sample chambers, they will destroy the lipid bilayer.

1. Fill two 3 mL syringes with Milli-Q water. Connect one of the syringes to the inlet port and push 1 mL of water through the flow cell. Connect the second syringe to the outlet port and push-pull the water between the inlet and outlet syringes to remove any air from the flow cell. Very small air bubbles may appear near the edge of the tape, but these are generally not problematic.
2. Mix 40 μL of liposome solution with 1 mL of lipid buffer (10 m*M* Tris-HCl [pH 8.0], 100 m*M* NaCl). Push 250 μL of the mixture into the flow cell approximately every 5 min until all of the liposome mixture is used. After the final injection, allow the lipids to form a cohesive bilayer by incubating at room temperature for 30 min.
3. Further passivate the surface with 1 mL of BSA buffer (40 m*M* Tris-HCl [pH 8.0], 2 m*M* $MgCl_2$, 1 m*M* DTT, and 0.2 mg/mL BSA). Incubate 5 min. The rolling circle replication reaction can be started at this time (see Section 2.3.2).
4. Mix 10 μL of streptavidin (1 mg/mL, Invitrogen, Cat. No. S888) with 790 μL of BSA buffer and push the solution through the sample chamber in two ~500 μL steps with a 5 min incubation between steps.
5. Rinse the sample chamber with 3 mL of BSA buffer to remove free streptavidin.
6. Dilute the freshly prepared rolling circle reaction with 450 μL of BSA buffer and slowly push the ssDNA solution through the sample chamber over a 10 min period. Mount the flow cell on the microscope stage and adjust the focus as necessary.
7. After mounting the flow cell on the microscope stage, the input and the output ports are connected to a sample injection system comprised of a syringe pump (KD Scientific, KDS-201) and a high-pressure switch valve (IDEX Health & Science, MXP9900–000). Again, it is essential that all connections be made using drop-to-drop connections to avoid inadvertently injecting air bubbles through the sample chamber.

2.3.4 Using RPA-eGFP to Visualize ssDNA—DNA curtains made with dsDNA can be visualized using an intercalating dye such as YOYO1. However, ssDNA is not readily labeled with intercalating dyes and the reactive oxygen species generated when these dyes are illuminated by laser light can rapidly nick the ssDNA, which is problematic because a single nick will result in release of the ssDNA from the flow cell surface. In addition, ssDNA forms extensive secondary structure, which must be removed in order to visualize extended molecules along their full contour lengths. To overcome these problems, we use a GFP-tagged version of the eukaryotic ssDNA-binding protein RPA both to label the ssDNA and to remove secondary structure so that the molecules can be easily extended by buffer flow (Fig. 5) (Gibb et al., 2012). RPA offers the additional benefit that RPA-coated ssDNA is the physiological substrate for assembly of the eukaryotic presynaptic complex (Bianco et al., 1998; Wold, 1997). The following steps outline a typical procedure for labeling and extending the ssDNA curtains with RPA-eGFP.

1. Begin by diluting an appropriate amount of *S. cerevisiae* RPA-eGFP into 20 mL of BSA buffer. RPA has a very high affinity for ssDNA (Wold, 1997), so working concentrations of just 0.1 n*M* RPA-eGFP are sufficient to label and extend the ssDNA.

2. Flush the RPA-containing buffer through the sample chamber at a rate of 1.0 mL/min for approximately 15 min. The ssDNA will immediately be visible by TIRFM upon injection of RPA-eGFP. The RPA-eGFP-ssDNA complexes initially appear as short molecules that slowly extend with time as secondary structure is removed (Fig. 5).

3. After 2 min of RPA buffer flow, a 500 μL pulse of 7 *M* urea is flushed through the sample chamber at 1 mL/min to help remove any residual ssDNA secondary structure, ϕ29 DNA polymerase, or M13 circular ssDNA template.

4. For double-tethering, a row of pentagon-shaped pedestals is lithographed downstream of the barriers (Fig. 2). These pedestals serve as anchor points for the nonspecific adsorption of the RPA-ssDNA, which stick to the exposed chromium surfaces. Nonspecific interactions between the downstream end of the RPA-ssDNA and the chromium pedestals allow the ssDNA to remain extended and visualized by TIRFM even in the absence of buffer flow.

2.3.5 Presynaptic Complex Assembly—The RPA-eGFP-coated ssDNA can serve as the starting point for assembly of the presynaptic complex, and we have used this as a substrate for the assembly of presynaptic complexes made from a variety of Rad51/RecA recombinases, including *Escherichia coli* RecA, *S. cerevisiae* Rad51, human Rad51, as well as the meiosis-specific recombinases *S. cerevisiae* Dmc1 and human Dmc1 (Lee et al., 2015; Qi et al., 2015). We use unlabeled Rad51/RecA recombinases for our experiments so successful assembly of the presynaptic complex is revealed by the displacement of the fluorescent RPA-eGFP (Fig. 6). Here, we briefly describe the procedure used for making an *S. cerevisiae* Rad51 presynaptic complex, but this protocol can be readily adapted for other Rad51/RecA recombinases.

1. Wash the RPA-eGFP-bound ssDNA curtains with HR buffer (30 m*M* Tris-Acetate [pH 7.5], 20 m*M* Mg-Acetate, 50 m*M* KCl, 1 m*M* DTT, 0.2 mg/mL BSA) plus 2.5 m*M* ATP for 2 min at a flow rate of 1 mL/min to remove any free RPA and equilibrate the sample chamber in HR buffer.

2. Inject a 50-μL sample of *S. cerevisiae* Rad51 (2 μ*M*) in HR buffer plus 2.5 m*M* ATP. Terminate buffer flow once Rad51 enters the sample chamber and incubate the sample in the absence of buffer flow for 15 min at 30°C.

3. Confirm assembly of the presynaptic complex by visual inspection of the ssDNA before, during, and after the Rad51 injection. Successful assembly of the presynaptic complex results in dissociation of RPA-eGFP from the ssDNA (Fig. 6). Once RPA-eGFP has been displaced from the ssDNA flush the sample chamber with additional HR buffer to remove any unbound Rad51.

4. The resulting Rad51 presynaptic complexes remain stable for at least 2 h if ATP is maintained in the buffer, and the stability of the complexes can be assessed using RPA-eGFP (Qi et al., 2015). RPA-eGFP will only bind to the ssDNA after dissociation of Rad51, so the integrity of the presynaptic complex can be readily confirmed by injecting HR buffer containing 0.1 n*M* RPA-eGFP (Fig. 6).

3. APPLICATIONS

Here, we briefly summarize some of the studies we have conducted using ssDNA curtains, which include analysis of RPA-binding dynamics, Rad51 presynaptic complex assembly, the association of protein cofactors with the Rad51 presynaptic complex, and interactions between the presynaptic complex and fluorescently tagged dsDNA fragments.

3.1 RPA-Binding Dynamics

RPA is a heterotrimeric complex composed of Rfa1, Rfa2, and Rfa3 subunits, and participates in all aspects of nucleic acid metabolism involving an ssDNA intermediate (Broderick, Rehmet, Concannon, & Nasheuer, 2010; Wold, 1997). RPA-ssDNA complexes are stable for over 2 h, without any detectable dissociation when free RPA is removed from solution (Gibb, Ye, Gergoudis et al., 2014; Gibb, Ye, Kwon, et al., 2014). However, the bound RPA can undergo rapid exchange when free RPA is present in solution, which can be visualized as a change in fluorescence color of the ssDNA when switching between RPA-eGFP and RPA-mCherry (Fig. 5C and D) (Deng, Gibb, de Almeida, Greene, & Symington, 2014; Gibb, Ye, Gergoudis et al., 2014; Gibb, Ye, Kwon, et al., 2014). This unusual behavior suggests that ssDNA-bound RPA undergoes constant microscopic dissociation under all conditions, but these microscopic dissociation events only result in macroscopically detectable dissociation into free solution when other ssDNA-binding proteins are present to compete with the transiently unbound species for exposed patches of ssDNA (Gibb, Ye, Gergoudis et al., 2014; Gibb, Ye, Kwon, et al., 2014). This concentration-dependent dissociation mechanism has been referred as facilitated dissociation (Ha, 2013), and it has now been reported for several different proteins (Cocco, Marko, & Monasson, 2014; Graham, Johnson, & Marko, 2011; Hadizadeh, Johnson, & Marko, 2016; Joshi et al., 2012; Kunzelmann, Morris, Chavda, Eccleston, & Webb, 2010), suggesting that facilitated dissociation may have a widespread impact on the turnover of nucleic acid-binding proteins.

3.2 Protein Cofactor Association with the Presynaptic Complex

ssDNA curtains can be used to monitor the assembly and disassembly of presynaptic complexes with either single- or double-tethered ssDNA molecules, and can also be used to determine how other HR proteins bind to the presynaptic complexes. For instance, Rad52 is a mediator protein that promotes assembly of the Rad51 presynaptic complex during the early stages of HR (Mortensen, Lisby, & Rothstein, 2009; Sung & Klein, 2006), and is also required for the second strand capture and strand annealing reactions that take place during the later stages of recombination (Lao, Oh, Shinohara, Shinohara, & Hunter, 2008; McIlwraith & West, 2008; Nimonkar & Kowalczykowski, 2009). We have used ssDNA curtains to study the spatial and temporal progression of RPA and Rad52 association with Rad51 during presynaptic complex assembly (Gibb, Ye, Gergoudis et al., 2014; Gibb, Ye,

Kwon, et al., 2014). These studies revealed that Rad52 can suppress RPA turnover, highlighting an unanticipated influence on protein dynamics, and also showed that both Rad52 and RPA can remain associated with the Rad51 presynaptic complex. As indicate earlier, there are ~45 different proteins that participate in DSB repair in *S. cerevisiae*, and in many instances we have only a cursory understanding of how these proteins function. Future studies using ssDNA curtains help reveal how these proteins interact with and influence the Rad51 presynaptic complex.

3.3 Duplex DNA Binding by the Presynaptic Complex

We have used ssDNA curtains along with short (70-bp) fluorescently tagged dsDNA molecules containing short tracts of sequence microhomology complementary to the presynaptic ssDNA to study processes that take place as *S. cerevisiae* Rad51, human Rad51, *S. cerevisiae* Dmc1, human Dmc1, and *E. coli* RecA presynaptic complexes are attempting to align and pair homologous DNA sequences (Lee et al., 2015; Qi et al., 2015). This work revealed that dsDNA sequences bearing fewer than 8-nucleotides (nts) of microhomology are rapidly sampled and rejected within seconds through a mechanism that gives rise to characteristic power law kinetics (Qi et al., 2015). However, dsDNA molecules bearing 8-nts of microhomology are more tightly bound, and the resulting intermediates exhibit single-exponential kinetics with lifetimes corresponding to tens of minutes (Fig. 7). Increasing the length of microhomology from 8- to 15-nt reveals changes in lifetimes that take place in 3-nt increments, suggesting that strand exchange takes place in 3-nt steps, with each step exhibiting a characteristic energetic signature that appears to be broadly conserved among the Rad51/RecA family members (Fig. 7) (Lee et al., 2015; Qi et al., 2015).

4. DATA COLLECTION AND ANALYSIS

In the following sections, we describe how to collect and analyze data from ssDNA curtain experiments using measurements of dsDNA binding to an unlabeled *S. cerevisiae* Rad51-ssDNA presynaptic complex as an example. Similar procedures can be used to study dsDNA-binding properties of other Rad51/RecA family members, or adapted to study interactions between the unlabeled presynaptic complexes and any fluorescently tagged protein or DNA component that binds to the presynaptic complex.

4.1 dsDNA Binding by the Rad51 Presynaptic Complex

To measure stable dsDNA binding, Rad51 presynaptic complexes are first prepared as described earlier (see Section 2.3.5). Atto565-tagged dsDNA oligonucleotides (10 n*M*) 70-bp in length are injected into the sample chamber in HR buffer (30 m*M* Tris-Acetate [pH 7.5], 20 m*M* Mg-Acetate, 50 m*M* KCl, 1 m*M* DTT, 0.2 mg/mL BSA) plus 2.5 m*M* ATP. Reactions are incubated for 10 min at 30°C in the absence of buffer flow and without laser illumination. The free dsDNA is removed by quickly flushing the sample chamber with HR buffer for 40 s at a flow rate of 1 mL/min. The flow rate is then reduced to 0.2 mL/min to allow continuous replenishment of ATP and removal of any dissociated dsDNA fragments. Data are acquired by capturing single 100 ms frames at either 20-, 30-, 40-, or 60-s intervals and the laser remains shuttered between each acquired image to minimize photobleaching. These measurements probe intermediates with lifetimes spanning a minute to tens of

minutes and the image acquisition frequency and overall duration of the experiments are adjusted to accommodate the lifetime of each particular dsDNA substrate. Kymographs are then generated from the resulting images as described later.

4.2 Generating Kymographs

Images are acquired through Nikon NIS Elements software and exported as individual tiff files for each exposure in the experiment. Using Fiji (ImageJ 1.48b, Wayne Rasband, National Institutes of Health, USA), the tiff files are stacked to create a tiff stack (i.e., movie) of the entire field of view. Kymographs representing individual presynaptic complexes are then generated from the resulting tiff stack using the "Reslice" function in Fiji. A straight line is superimposed on an ssDNA molecule and the corresponding image information for every image within the tiff stack is compiled as a new image. Each resulting kymograph represents a two-dimension projection of the events relating to a single presynaptic complex over the course of a reaction trajectory-the *y*-component reflects the position information and *x*-component represents time (Figs. 5–7). The resulting kymographs can then be used to assess the dsDNA-binding distributions, as previously described (Qi et al., 2015), as well as the lifetimes of fluorescent molecules bound to the presynaptic complex (see later) (Lee et al., 2015; Qi et al., 2015).

4.3 Survival Probability

Dissociation kinetics are analyzed by measuring the amount of time (dwell time) that each molecule of Atto565-labeled dsDNA remained bound to the Rad51-ssDNA presynaptic complexes after flushing the unbound dsDNA from the sample chamber (Fig. 7A–C). Survival probability analysis allows one to extract lifetime information for the labeled dsDNA fragments bound to the unlabeled presynaptic complex. Multiple kymographs are first analyzed manually to determine the lifetime of each individual binding event that is observed within the kymographs (Fig. 7B). These lifetimes are then plotted from shortest to longest and the resulting curves are analyzed to extract dissociation parameters. For a simple dissociation process, the distribution of lifetimes is expected to resemble a single-exponential decay. The probability of survival at time t is then defined as the proportion of molecules that remain bound to the ssDNA at time t, which can be defined as the number of molecules whose lifetime exceeds a particular time point, divided by the total number of observed binding events (Fig. 7D).

Bootstrapping is a standard statistic method used to estimate confidence intervals of a population mean by randomly resampling a subset of data from within a larger data set (Efron & Tibshirani, 1993). Error bars for the survival probability measurements are then expressed as 70% confidence intervals obtained through this bootstrap analysis. Use of 70% confidence intervals for the bootstrapped data provides a close approximation to expectations for one standard deviation from the mean because for any normally distributed data set 68.27% of the values lie within one standard deviation of the mean.

4.4 Free Energy Changes During Base Triplet Stepping

Survival curves generated from experiments using the 70-bp dsDNA substrates bearing 8–15-nts of microhomology (Fig. 7C) can be fitted to a simple exponential decay function of

the form e^{-kt}, where k is the experimentally observed dissociation rate constant and t is time (Fig. 7D). This observed dissociation rate constant is comprised of two components: the actual dsDNA dissociation rate constant and the Atto565 photobleaching rate constant. Subtracting photobleaching rate, which must be determined separately (Qi et al., 2015), from the experimentally observed dissociation rate k allows one to determine the actual dissociation constant for the dsDNA substrates (k_d). The Arrhenius equation can then be used to relate the experimentally determined k_d to the free energy barrier ($\Delta G^{\ddagger}$) for dsDNA binding as follows:

$$k_d = Ae^{-\frac{\Delta G^{\ddagger}}{k_b T}},$$

where A is the jump frequency, k_b is the Boltzmann constant, and T is temperature (Qi et al., 2015). The difference in the barrier heights ($\Delta\Delta G^{\ddagger}$) between two different dsDNA substrates can then be compared using the following relation:

$$\Delta\Delta G^{\ddagger} = \Delta G_2^{\ddagger} - \Delta G_1^{\ddagger} = k_b T \ln \frac{k_d^1}{k_d^2}$$

These $\Delta\Delta G^{\ddagger}$ values can be normalized such that $\Delta G^{\ddagger}$ for a dsDNA substrate containing a single 8-nt tract of microhomology is set to zero, and all other $\Delta\Delta G^{\ddagger}$ values for dsDNA fragments harboring longer lengths of microhomology are expressed relative to the substrate bearing 8-nts of microhomology (Fig. 7E) (Lee et al., 2015).

4.5 Real-Time Binding Measurements

The experiments described earlier pertain to relatively stable reaction intermediates with lifetimes on the order of tens of minutes. However, less stable intermediates can also be readily detected by increasing the data acquisition frequency. For instance, transient dsDNA sampling by the Rad51-ssDNA presynaptic complex can be detected over much shorter time regimes (Qi et al., 2015). This is accomplished by injecting the Atto565-tagged dsDNA substrate (10 n*M*) into a sample chamber containing assembled presynaptic complexes. Buffer flow is then terminated without flushing away the free dsDNA and images are acquired with 60 ms exposure time using continuous laser illumination in the absence of shuttering. The resulting data for the transient binding intermediates can then be analyzed as described earlier based on kymographs generated from the resulting tiff stacks. The dwell times for each binding event are then defined as the difference between the first frame and the last frame in which a particular molecule of Atto565-labeled dsDNA is observed bound to the Rad51 presynaptic complex. The data describing all of the transient dsDNA-binding events are then synchronized such that the initial appearance of each bound Atto565-DNA was defined as time zero, and then the probability that a bound molecule survived up to a particular time point (t) was determined as the fraction of Atto565-DNA molecules that remained bound at time t. Survival probability graphs can then constructed from the resulting data to analyze dwell times, as described earlier for the more stable dsDNA-binding intermediates.

5. CONCLUSION AND FUTURE DIRECTIONS

ssDNA curtains provide a powerful experimental platform, enabling new avenues of investigation into the biochemical and biophysical properties of Rad51/RecA-ssDNA presynaptic complexes. These studies offer the potential for new insights into the assembly, stability, and regulation of this crucial HR intermediate, and the procedures described here can be adapted to study many different questions related to HR. Future ssDNA curtains studies may help provide additional insights into the DNA transactions that take place during HR, and may also provide important new clues into the dozens of other proteins that are necessary for HR to take place within living cells. Of particular interest will be work looking at how nucleosomes and chromatin impact the interactions of the Rad51-ssDNA presynaptic complex with dsDNA, and how these interactions are modulated by nucleosome-remodeling proteins and posttranslational histone modifications. In addition, these ssDNA curtain methods can be adapted for studies involving other types of ssDNA-binding proteins, and with additional development it may even be possible to extend these research tools to study of single-stranded RNA substrates.

ACKNOWLEDGMENTS

We thank Corentin Moevus, Daniel Duzdevich, Johannes Stigler, and Luisina De Tullio for comments on the manuscript. This research was funded by NIH Grants GM082848 (E.C.G.), GM074739 (E.C.G.), and F31CA210663 (J.B.S.), and by the National Science Foundation Grant MCB1154511 (E.C.G.).

REFERENCES

Axelrod D (1989). Total internal reflection fluorescence microscopy. Methods in Cell Biology, 30, 245–270. [PubMed: 2648112]

Bianco PR, Tracy RB, & Kowalczykowski SC (1998). DNA strand exchange proteins: A biochemical and physical comparison. Frontiers in Bioscience, 3, D570–D603. [PubMed: 9632377]

Broderick S, Rehmet K, Concannon C, & Nasheuer HP (2010). Eukaryotic single-stranded DNA binding proteins: Central factors in genome stability. Sub-cellular Biochemistry, 50, 143–163. [PubMed: 20012581]

Chen Z, Yang H, & Pavletich NP (2008). Mechanism of homologous recombination from the RecA-ssDNA/dsDNA structures. Nature, 453, 489–494. [PubMed: 18497818]

Cocco S, Marko JF, & Monasson R (2014). Stochastic ratchet mechanisms for replacement of proteins bound to DNA. Physical Review Letters, 112, 238101. [PubMed: 24972228]

Conway AB, Lynch TW, Zhang Y, Fortin GS, Fung CW, Symington LS, et al. (2004). Crystal structure of a Rad51 filament. Nature Structural and Molecular Biology, 11, 791–796.

Cromie GA, Connelly JC, & Leach DR (2001). Recombination at double-strand breaks and DNA ends: Conserved mechanisms from phage to humans. Molecular Cell, 8, 1163–1174. [PubMed: 11779493]

Deng SK, Gibb B, de Almeida MJ, Greene EC, & Symington LS (2014). RPA antagonizes microhomology-mediated repair of DNA double-strand breaks. Nature Structural and Molecular Biology, 21, 405–412.

Duzdevich D, Warner MD, Ticau S, Ivica NA, Bell SP, & Greene EC (2015). The dynamics of eukaryotic replication initiation: Origin specificity, licensing, and firing at the single-molecule level. Molecular Cell, 58, 483–494. [PubMed: 25921072]

Efron B, & Tibshirani R (1993). An introduction to the bootstrap. New York: Champman and Hall, Inc.

Fazio T, Visnapuu ML, Wind S, & Greene EC (2008). DNA curtains and nanoscale curtain rods: High-throughput tools for single molecule imaging. Langmuir, 24, 10524–10531. [PubMed: 18683960]

Game JC, & Mortimer RK (1974). A genetic study of X-ray sensitive mutants in yeast. Mutation Research, 24, 281–292. [PubMed: 4606119]

Gibb B, Silverstein TD, Finkelstein IJ, & Greene EC (2012). Single-stranded DNA curtains for real-time single-molecule visualization of protein-nucleic acid interactions. Analytical Chemistry, 84, 7607–7612. [PubMed: 22950646]

Gibb B, Ye LF, Gergoudis SC, Kwon Y, Niu H, Sung P, et al. (2014a). Concentration-dependent exchange of replication protein A on single-stranded DNA revealed by single-molecule imaging. PloS One, 9, e87922. [PubMed: 24498402]

Gibb B, Ye LF, Kwon Y, Niu H, Sung P, & Greene EC (2014b). Protein dynamics during presynaptic-complex assembly on individual single-stranded DNA molecules. Nature Structural & Molecular Biology, 21, 893–900.

Gorman J, Fazio T, Wang F, Wind S, & Greene EC (2010). Nanofabricated racks of aligned and anchored DNA substrates for single-molecule imaging. Langmuir, 26, 1372–1379. [PubMed: 19736980]

Gorman J, Plys AJ, Visnapuu ML, Alani E, & Greene EC (2010). Visualizing one-dimensional diffusion of eukaryotic DNA repair factors along a chromatin lattice. Nature Structural and Molecular Biology, 17, 932–938.

Gorman J, Wang F, Redding S, Plys AJ, Fazio T, Wind S, et al. (2012). Single-molecule imaging reveals target-search mechanisms during DNA mismatch repair. Proceedings of the National Academy of Sciences of the United States of America, 109, E3074–E3083. [PubMed: 23012240]

Graham JS, Johnson RC, & Marko JF (2011). Concentration-dependent exchange accelerates turnover of proteins bound to double-stranded DNA. Nucleic Acids Research, 39, 2249–2259. [PubMed: 21097894]

Graneli A, Yeykal CC, Prasad TK, & Greene EC (2006). Organized arrays of individual DNA molecules tethered to supported lipid bilayers. Langmuir, 22, 292–299. [PubMed: 16378434]

Greene EC, Wind S, Fazio T, Gorman J, & Visnapuu ML (2010). DNA curtains for high-throughput single-molecule optical imaging. Methods in Enzymology, 472, 293–315. [PubMed: 20580969]

Ha T (2013). Single-molecule approaches embrace molecular cohorts. Cell, 154, 723–726. [PubMed: 23953107]

Haber JE (2012). Mating-type genes and MAT switching in Saccharomyces cerevisiae. Genetics, 191, 33–64. [PubMed: 22555442]

Hadizadeh N, Johnson RC, & Marko JF (2016). Facilitated dissociation of a nucleoid protein from the bacterial chromosome. Journal of Bacteriology, 198, 1735–1742. [PubMed: 27044624]

Heyer WD, Ehmsen KT, & Liu J (2010). Regulation of homologous recombination in eukaryotes. Annual Review of Genetics, 44, 113–139.

Joshi CP, Panda D, Martell DJ, Andoy NM, Chen TY, Gaballa A, et al. (2012). Direct substitution and assisted dissociation pathways for turning off transcription by a MerR-family metalloregulator. Proceedings of the National Academy of Sciences of the United States of America, 109, 15121–15126. [PubMed: 22949686]

Kunzelmann S, Morris C, Chavda AP, Eccleston JF, & Webb MR (2010). Mechanism of interaction between single-stranded DNA binding protein and DNA. Biochemistry, 49, 843–852. [PubMed: 20028139]

Lao JP, Oh SD, Shinohara M, Shinohara A, & Hunter N (2008). Rad52 promotes postinvasion steps of meiotic double-strand-break repair. Molecular Cell, 29, 517–524. [PubMed: 18313389]

Lee JY, Finkelstein IJ, Arciszewska LK, Sherratt DJ, & Greene EC (2014). Single-molecule imaging of FtsK translocation reveals mechanistic features of protein-protein collisions on DNA. Molecular Cell, 54, 832–843. [PubMed: 24768536]

Lee JY, Terakawa T, Qi Z, Steinfeld JB, Redding S, Kwon Y, et al. (2015). DNA recombination. Base triplet stepping by the Rad51/RecA family of recombinases. Science, 349, 977–981. [PubMed: 26315438]

Lisby M, & Rothstein R (2009). Choreography of recombination proteins during the DNA damage response. DNA Repair, 8, 1068–1076. [PubMed: 19473884]

Lisby M, & Rothstein R (2015). Cell biology of mitotic recombination. Cold Spring Harbor Perspectives in Biology, 7, a016535. [PubMed: 25731763]

McIlwraith MJ, & West SC (2008). DNA repair synthesis facilitates RAD52-mediated second-end capture during DSB repair. Molecular Cell, 29, 510–516. [PubMed: 18313388]

Mine-Hattab J, & Rothstein R (2013). DNA in motion during double-strand break repair. Trends in Cell Biology, 23, 529–536. [PubMed: 23867212]

Morrical SW (2015). DNA-pairing and annealing processes in homologous recombination and homology-directed repair. Cold Spring Harbor Perspectives in Biology, 7, a016444. [PubMed: 25646379]

Mortensen UH, Lisby M, & Rothstein R (2009). Rad52. Current Biology, 19, R676–R677. [PubMed: 19706272]

Nimonkar AV, & Kowalczykowski SC (2009). Second-end DNA capture in double-strand break repair: How to catch a DNA by its tail. Cell Cycle, 8, 1816–1817. [PubMed: 19471119]

Paques F, & Haber JE (1999). Multiple pathways of recombination induced by double-strand breaks in Saccharomyces cerevisiae. Microbiology and Molecular Biology Reviews, 63, 349–404. [PubMed: 10357855]

Qi Z, Redding S, Lee JY, Gibb B, Kwon Y, Niu H, et al. (2015). DNA sequence alignment by microhomology sampling during homologous recombination. Cell, 160, 856–869. [PubMed: 25684365]

Redding S, Sternberg SH, Marshall M, Gibb B, Bhat P, Guegler CK, et al. (2015). Surveillance and processing of foreign DNA by the *Escherichia coli* CRISPR-Cas system. Cell, 163, 854–865. [PubMed: 26522594]

San Filippo J, Sung P, & Klein H (2008). Mechanism of eukaryotic homologous recombination. Annual Review of Biochemistry, 77, 229–257.

Sasaki M, Lange J, & Keeney S (2010). Genome destabilization by homologous recombination in the germ line. Nature Reviews. Molecular Cell Biology, 11, 182–195. [PubMed: 20164840]

Silverstein TD, Gibb B, & Greene EC (2014). Visualizing protein movement on DNA at the single-molecule level using DNA curtains. DNA Repair, 20, 94–109. [PubMed: 24598576]

Sternberg SH, Redding S, Jinek M, Greene EC, & Doudna JA (2014). DNA interrogation by the CRISPR RNA-guided endonuclease Cas9. Nature, 507, 62–67. [PubMed: 24476820]

Sung P, & Klein H (2006). Mechanism of homologous recombination: Mediators and helicases take on regulatory functions. Nature Reviews. Molecular Cell Biology, 7, 739–750. [PubMed: 16926856]

Symington LS, Rothstein R, & Lisby M (2014). Mechanisms and regulation of mitotic recombination in Saccharomyces cerevisiae. Genetics, 198, 795–835. [PubMed: 25381364]

Wang F, Redding S, Finkelstein IJ, Gorman J, Reichman DR, & Greene EC (2013). The promoter-search mechanism of *Escherichia coli* RNA polymerase is dominated by three-dimensional diffusion. Nature Structural and Molecular Biology, 20, 174–181.

Wold MS (1997). Replication protein A: A heterotrimeric, single-stranded DNA-binding protein required for eukaryotic DNA metabolism. Annual Review of Biochemistry, 66, 61–92.

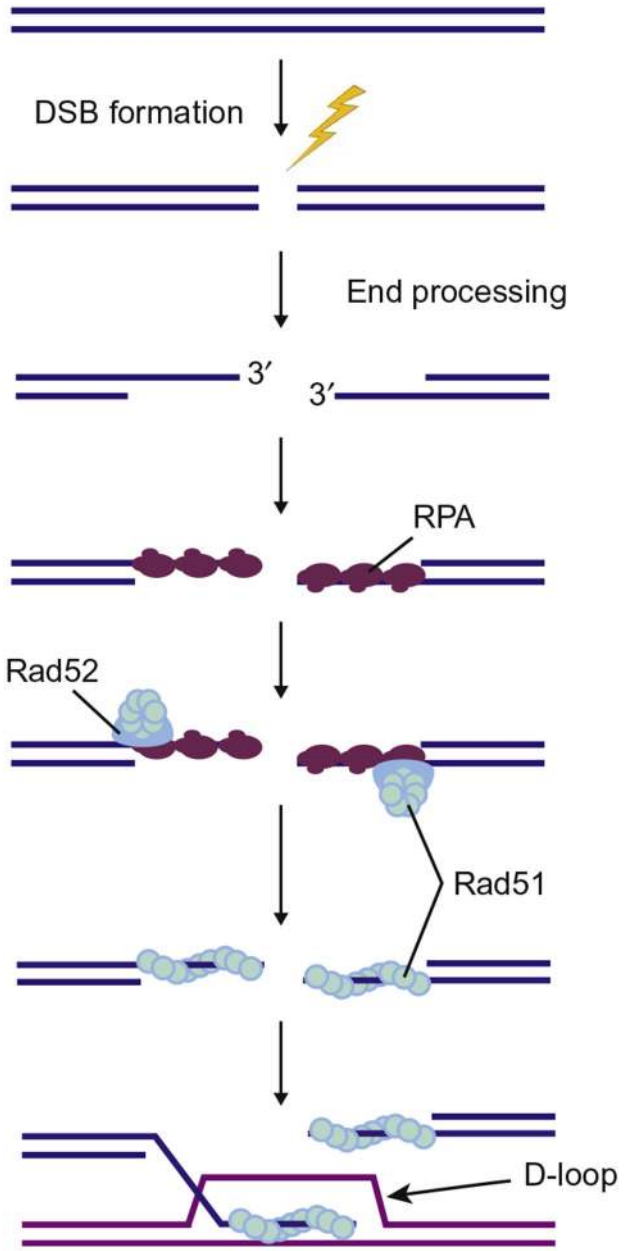

Fig. 1.

Early stages of eukaryotic homologous recombination. DSBs are resected to yield long 3′ ssDNA overhangs that are first bound by RPA. Rad52 then binds and assists loading of the Rad51, which forms long filaments on the ssDNA and these Rad51-ssDNA filaments are referred to as the presynaptic complex. The presynaptic complex then searches for a homologous DNA and pairs the processed ssDNA overhang with its homologous partner to generate a D-loop intermediate.

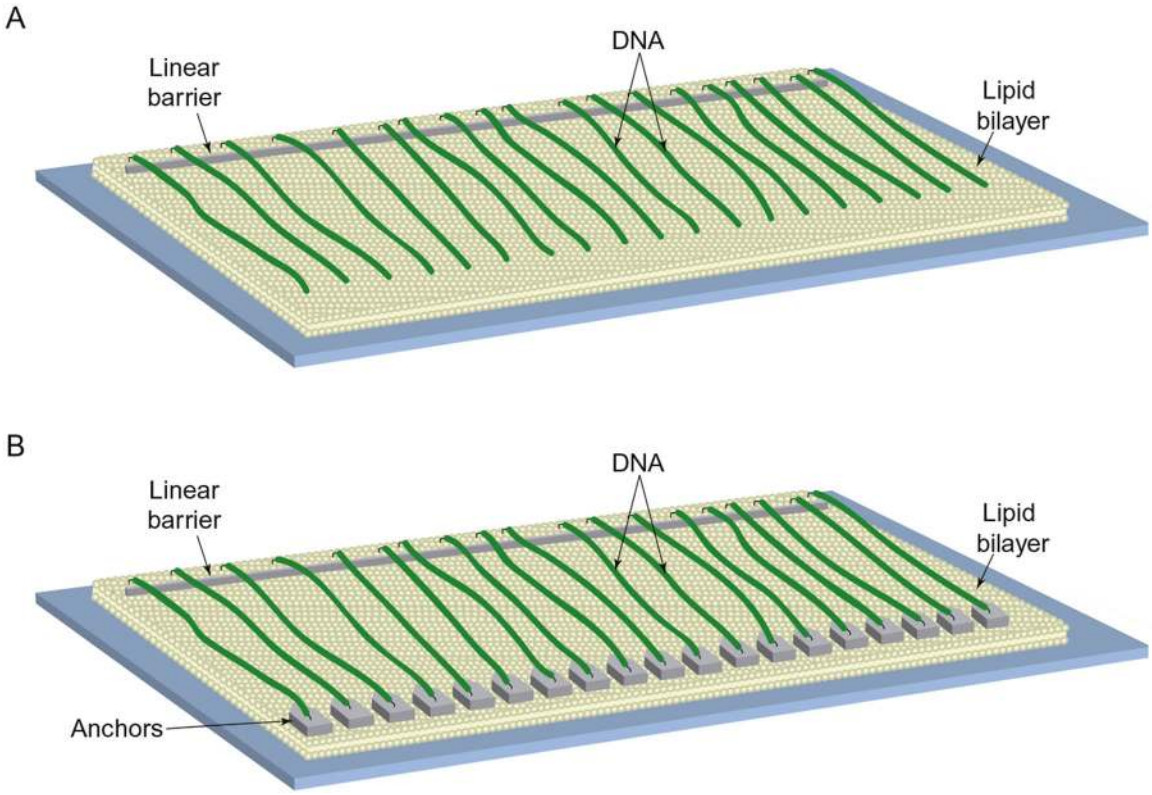

Fig. 2.

Different types of DNA curtains. (A) Schematic illustration of a single-tethered DNA curtain made with a linear barrier. (B) Double-tethered DNA curtain where the downstream ends of the DNA are tethered to the exposed anchor points that project above the bilayer. Both formats are compatible with either dsDNA or ssDNA. *Adapted with permission from* Silverstein, T. D., Gibb, B., & Greene, E. C. (2014). *Visualizing protein movement on DNA at the single-molecule level using DNA curtains*. DNA Repair (Amst), 20, *94–109*.

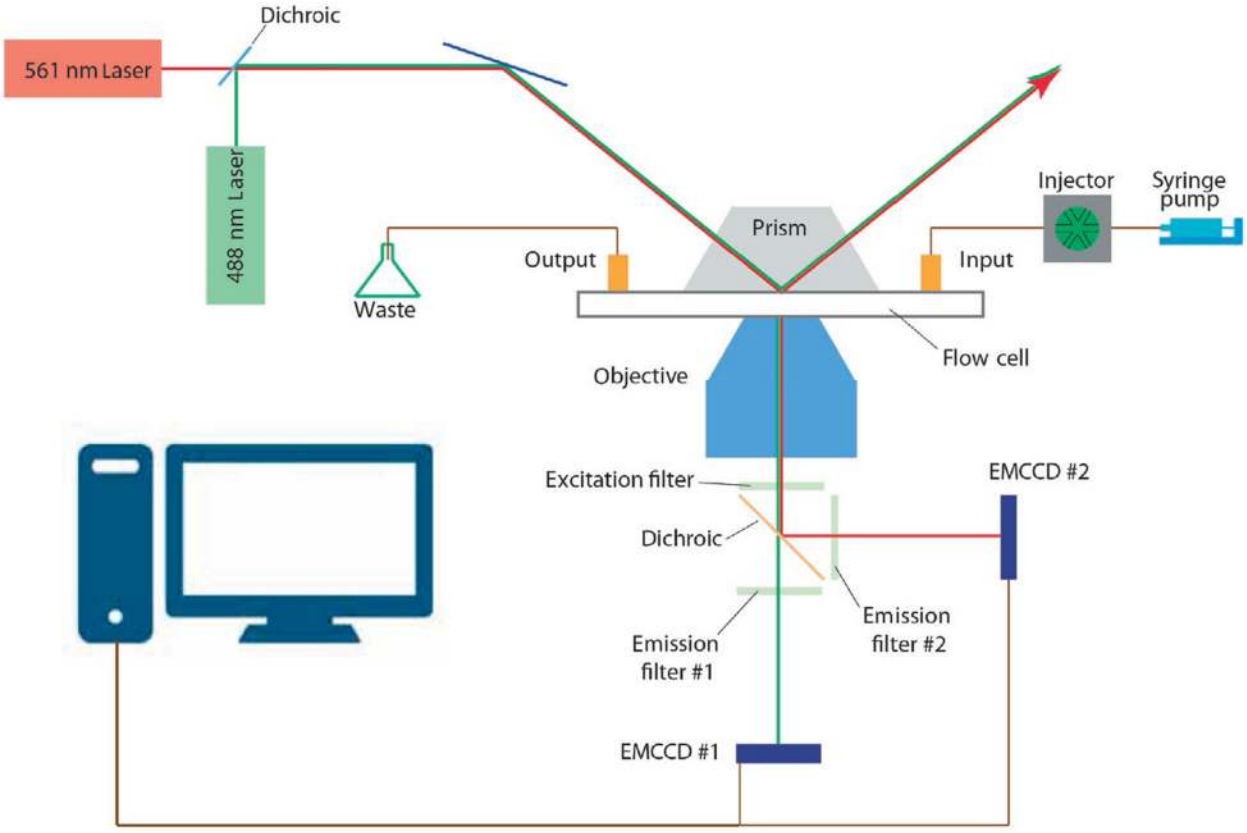

Fig. 3.

Total internal reflection fluorescence microscopy. This schematic highlights important details of the TIRFM systems used to visualize DNA curtains. Details of the schematic and system components are presented in the main text.

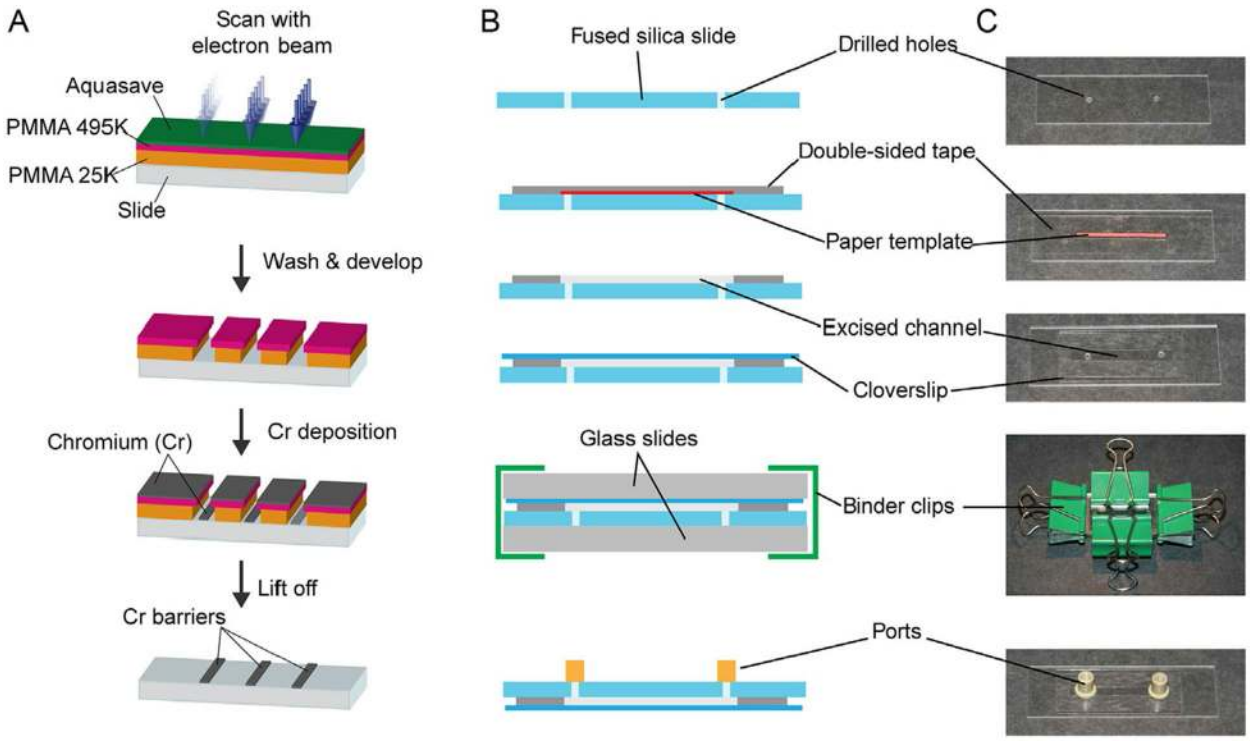

Fig. 4.

Flow cell fabrication. (A) Slides are first coated with two layers of PMMA, a layer of AquaSAVE, and an electron beam is then used to etch through these layers. Chromium is deposited on the surface and the remaining PMMA is removed, leaving behind the nanofabricated barriers. Schematic illustrations (B) and photographs (C) depicting the different stages of flow cell assembly. *Adapted with permission from* Greene, E. C., Wind, S., Fazio, T., Gorman, J., & Visnapuu, M. L. (2010). *DNA curtains for high-throughput single-molecule optical imaging*. Methods in Enzymology, 472, *293–315*.

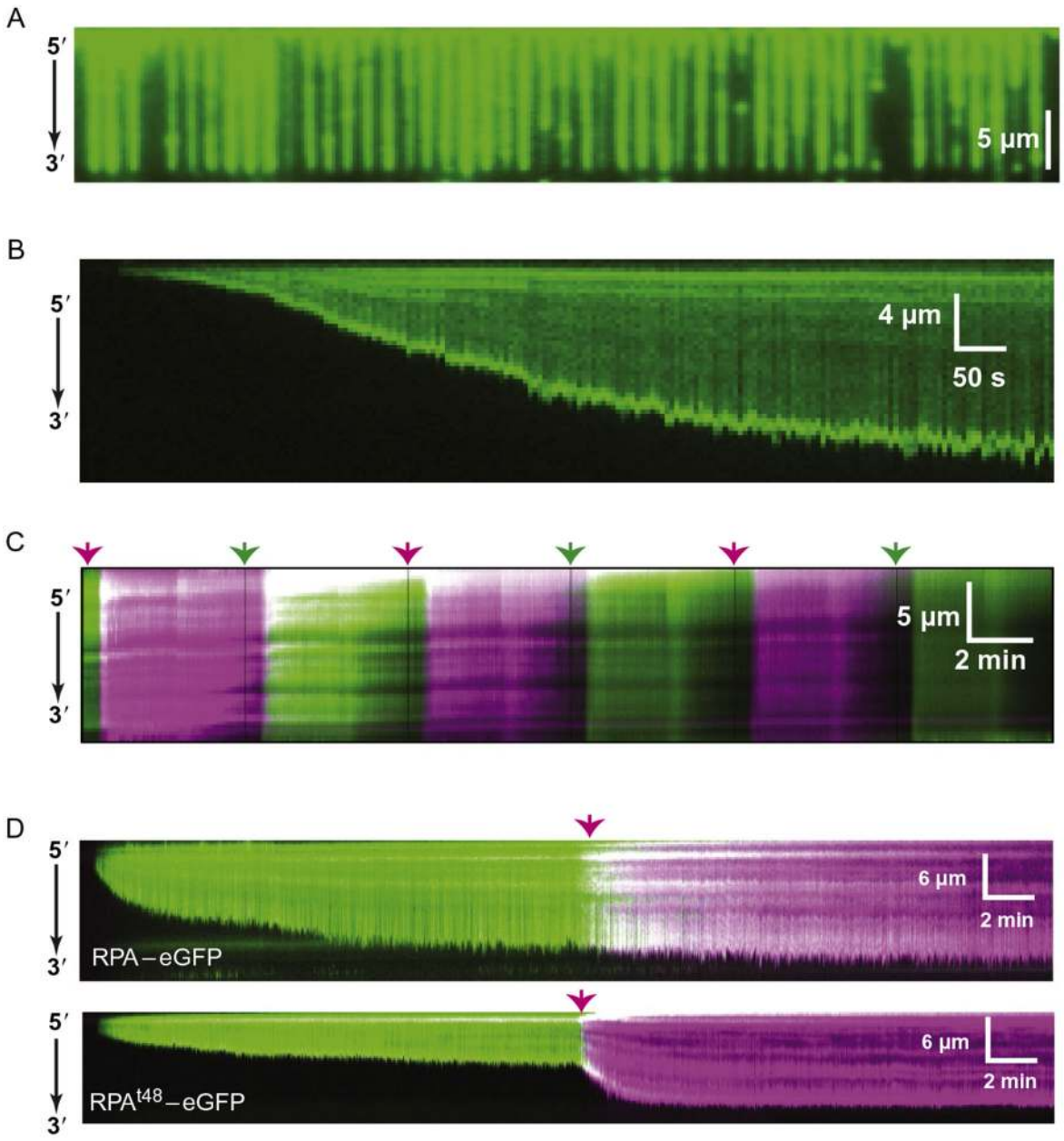

Fig. 5.

RPA-coated ssDNA curtains. (A) Wide-field TIRFM image of a double-tethered ssDNA curtain bound by RPA-eGFP. (B) Kymograph showing what takes place when single-tethered ssDNA molecules are labeled with RPA-eGFP. The ssDNA slowly becomes longer as RPA-eGFP binds and disrupts existing secondary structure. (C) Kymograph showing facilitated dissociation of RPA from the ssDNA when free RPA is injected into the sample chamber. RPA-eGFP is shown in *green*, and RPA-mCherry is shown in *magenta*, and the *color-coded arrowheads* indicate successive injections of each protein. (D) Kymographs of a single-tethered ssDNA showing that the exchange of wild-type RPA-eGFP with wild-type RPA-mCherry does not alter ssDNA length (*upper panel*), whereas exchange of the RPA^{t48} mutant, which is defective for ssDNA binding, with wild-type RPA-mCherry coincides with

an increase in ssDNA length. *Adapted with permission from* Deng, S. K., Gibb, B., de Almeida, M. J., Greene, E. C., & Symington, L. S. (2014). *RPA antagonizes microhomology-mediated repair of DNA double-strand breaks*. Nature Structural and Molecular Biology, 21, *405–412*; Gibb, B., Silverstein, T. D., Finkelstein, I. J., & Greene, E. C. (2012). *Single-stranded DNA curtains for* real-time single-molecule visualization of protein-nucleic acid interactions, *Analytical Chemistry*, *84*, 7607–7612; Gibb, B., Ye, L. F., Gergoudis, S. C., Kwon, Y., Niu, H., Sung, P., et al. (2014). Concentration-dependent exchange of replication protein A on single-stranded DNA revealed by single-molecule imaging. *PloS One*, *9*, e87922; Gibb, B., Ye, L. F., Kwon, Y., Niu, H., Sung, P., & Greene, E. C. (2014). Protein dynamics during presynaptic-complex assembly on individual single-stranded DNA molecules. *Nature Structural and Molecular Biology*; and Qi, Z., Redding, S., Lee, J. Y., Gibb, B., Kwon, Y., Niu, H., et al. (2015). DNA sequence alignment by microhomology sampling during homologous recombination. *Cell*, *160*, 856–869.

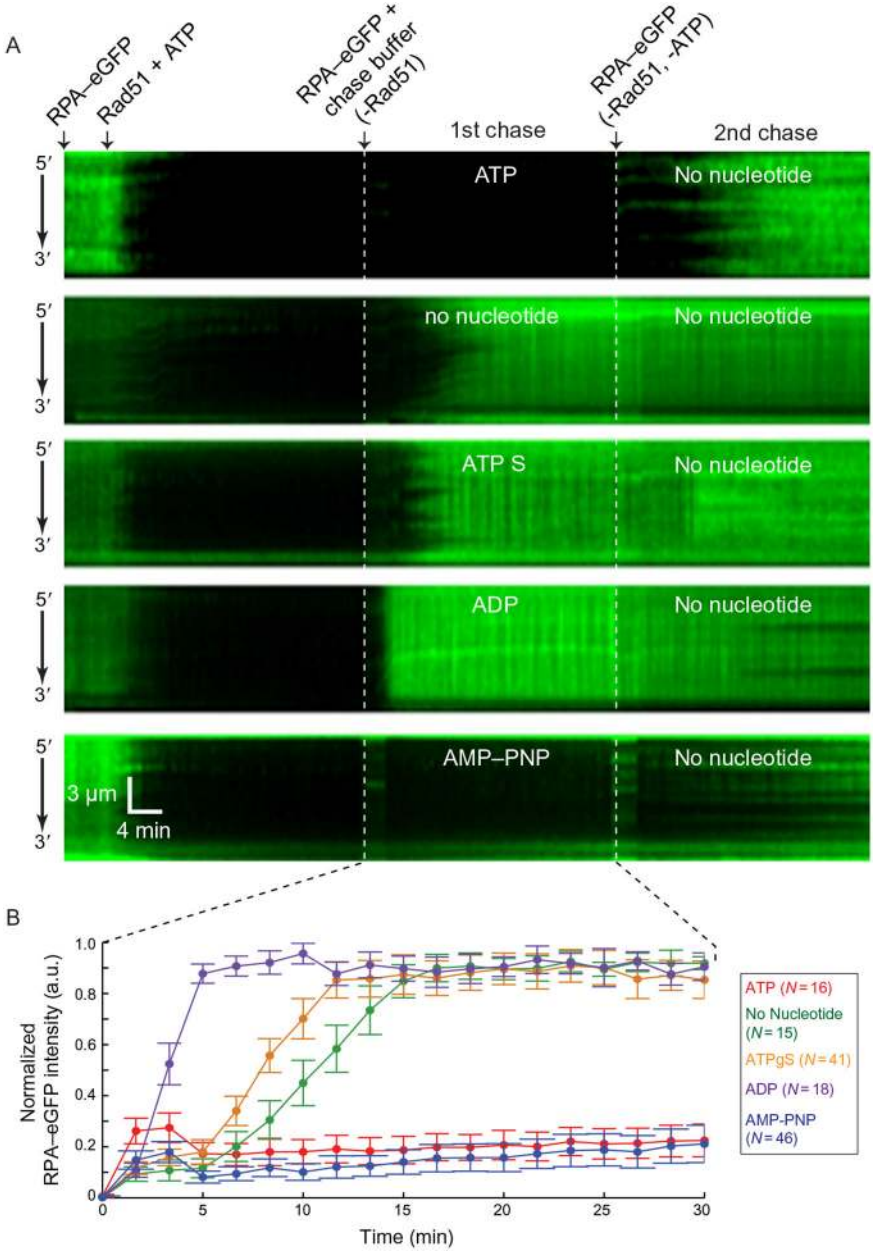

Fig. 6.

Kymographs showing presynaptic complex assembly reactions. (A) RPA-eGFP-ssDNA curtains were first incubated with 1 μ*M S. cerevisiae* wild-type (unlabeled) Rad51 and 2.5 m*M* ATP. Binding of Rad51 to the ssDNA is revealed as a rapid loss of RPA-eGFP fluorescence signal. The sample chambers were then flushed (1st chase) with buffer containing 1.0 n*M* RPA-eGFP and either no nucleotide or 2.5 m*M* of the indicated nucleotide cofactor, followed by a 30-min incubation. Disassembly of the Rad51-ssDNA presynaptic filaments is revealed by the binding of RPA-eGFP to the exposed ssDNA. The sample chambers were then flushed (2nd chase) with additional buffer containing 0.1 n*M* RPA-eGFP and no nucleotide cofactor, and incubated for an additional 30-min. (B) Quantitation of the Rad51 filament stability in the presence of various nucleotide cofactors,

as indicated. *Error bars* represent s.d. *Adapted with permission from* Qi, Z., Redding, S., Lee, J. Y., Gibb, B., Kwon, Y., Niu, H., et al. (2015). *DNA sequence alignment by microhomology sampling during homologous recombination*. Cell, 160, *856–869*.

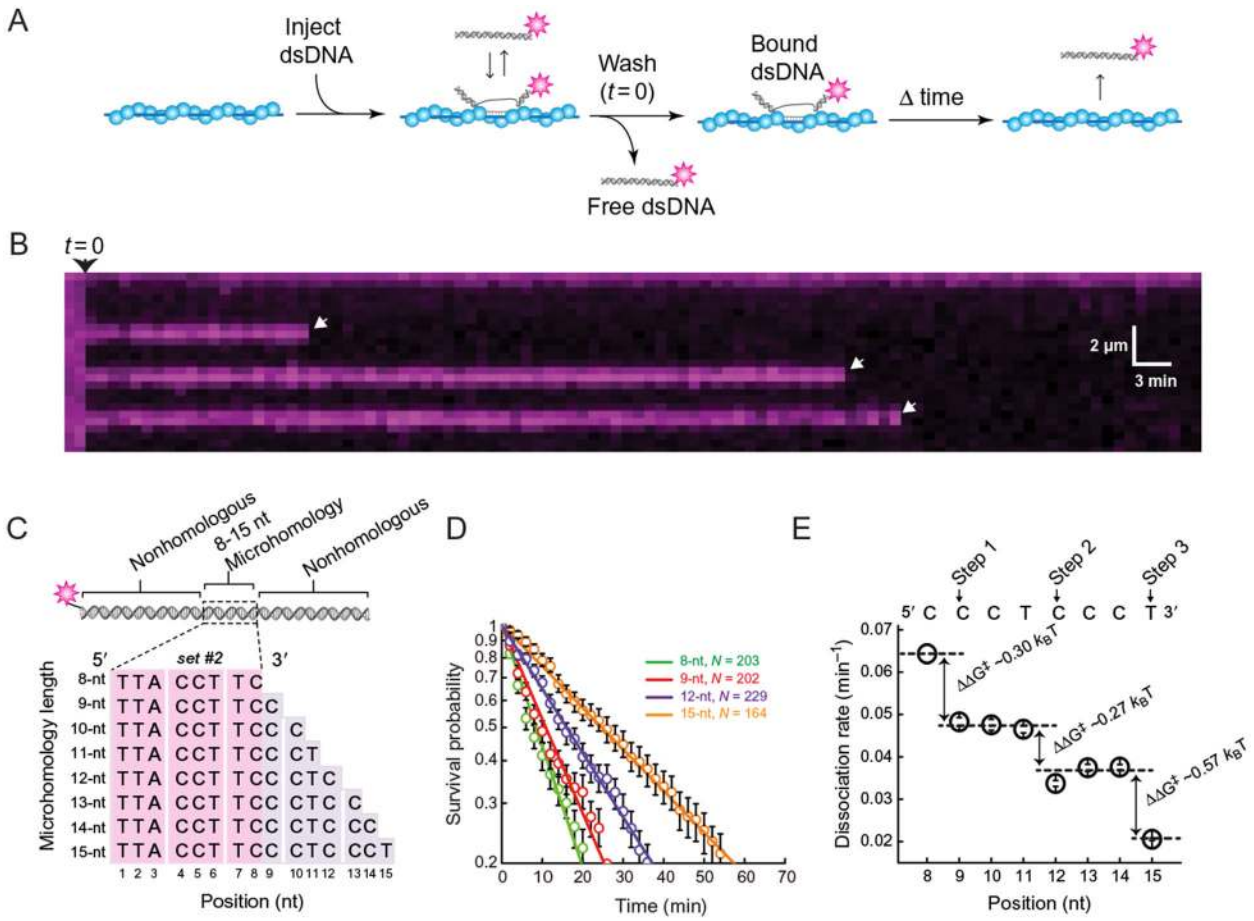

Fig. 7.

Duplex DNA binding by the *S. cerevisiae* Rad51 presynaptic complex. (A) Experimental schematic for measuring the survival probability of fluorescently tagged dsDNA oligonucleotides bound the presynaptic complex. (B) Example of a kymograph showing the binding of single Atto565-dsDNA molecules to a ScRad51 presynaptic complex. *White arrowheads* highlight individual dsDNA dissociation events. (C) Schematic of the 70-bp dsDNA substrates. All substrates contain an internal 8- to 15-nt tract of microhomology (as indicated) flanked by nonhomologous sequence. (D) Survival probability data for substrates with 8- to 15-nt of microhomology, as indicated; survival probability curves for the 10- and 11-nt substrates superimpose with the 9-nt and are omitted for clarity, and the 13- and 14-nt substrates superimpose 12-nt data sets and are also omitted for clarity. Data were analyzed by measuring the amount of time (dwell time) that each Atto565-DNA molecule remained bound to the Rad51-ssDNA presynaptic complexes after flushing unbound DNA from the sample chamber. (E) Atto565-dsDNA dissociation rates (mean ± s.d.) for reactions with *S. cerevisiae* Rad51 in the presence of AMP-PNP. Each data point was calculated from an average of ~150 molecules (N=70–250). *Arrows* indicate stepwise reductions in dissociation rates coincident with recognition of the 3rd base of each triplet, dashed lines report the mean rate for each step, and the free energy changes ($\Delta\Delta G^{\ddagger}$) associated with each triplet step are indicated. *Adapted with permission from* Lee, J. Y., Terakawa, T., Qi, Z., Steinfeld, J. B.,

Redding, S., Kwon, Y., et al. (2015). *DNA recombination. Base triplet stepping by the Rad51/RecA family of recombinases*. Science, 349, *977–981*.